

# QUANTIFYING AND CONTROLLING BIASES IN DARK MATTER HALO CONCENTRATION ESTIMATES

C. N. POVEDA-RUIZ<sup>1</sup> J. E. FORERO-ROMERO<sup>1</sup> J. C. MUÑOZ-CUARTAS<sup>2</sup>

<sup>1</sup>Departamento de Física, Universidad de los Andes, Cra. 1 No. 18A-10, Edificio Ip, Bogotá, Colombia

<sup>2</sup>Instituto de Física - FCEN, Universidad de Antioquia, Calle 67 No. 53-108, Medellín, Colombia

*Submitted for publication in ApJL*

## ABSTRACT

We use bootstrapping to estimate the bias of concentration estimates on N-body dark matter halos as a function of particle number. We find that algorithms based on the maximum radial velocity and radial particle binning tend to overestimate the concentration by 15% – 20% for halos sampled with 200 particles and by 7%-10% for halos sampled with 500 particles. To control this bias at low particle numbers we propose a new algorithm that estimates halo concentrations based on the integrated mass profile. The method uses the full particle information without any binning, making it reliable in cases when low numerical resolution becomes a limitation for other methods. This method reduces the bias to  $< 3\%$  for halos sampled with 200-500 particles. The velocity and density methods have to use halos with least  $\sim 4000$  particles in order to keep the biases down to the same low level. We also show that the mass-concentration relationship could be shallower than expected once the biases of the different concentration measurements are taken into account. These results show that bootstrapping and the concentration estimates based on the integrated mass profile are valuable tools to probe the internal structure of dark matter halos in numerical simulations.

*Subject headings:* Galaxies: halos — Dark matter — Methods: numerical

## 1. INTRODUCTION

In the current structure formation paradigm the properties of galaxies are coupled to the evolution of their dark matter (DM) hosting halo. In this paradigm the sizes and dynamics of galaxies are driven by the halo internal DM distribution.

The internal DM distribution in a halo is usually parameterized through the density profile. In a first approximation this profile is spherically symmetric; the density only depends on the radial coordinate. One of the most popular radial parameterizations is the Navarro-Frenk-White (NFW) profile (Navarro et al. 1997). This profile can be considered as universal (Navarro et al. 2010), assuming that one is not interested in the very central region where galaxy formation takes place, and where the effects of baryon physics on the dark matter distribution are still unknown. This profile is a double power law in radius, where the transition break happens at the so-called scale radius,  $r_s$ . The ratio between the scale radius and the halo virial radius  $R_v$  is known as the concentration  $c = R_v/r_s$ .

The concentration of the NFW profile provides a conceptual framework to study simulated dark matter halos as a function of redshift and cosmological parameters. Numerical studies (Neto et al. 2007; Macciò et al. 2008; Duffy et al. 2008; Muñoz-Cuartas et al. 2011; Prada et al. 2012; Ludlow et al. 2014, 2016; Klypin et al. 2016) summarized their results through the mass-concentration relationship; that is, the distribution of concentration values at a fixed halo mass and redshift. The success of such numerical experiments rests on a reliable algorithm to estimate the concentration. Such an algorithm should provide unbiased results and must be robust when applied at varying numerical resolution.

There are two established algorithms to estimate the concentration parameter. The first method takes the

halo particles and bins them into logarithmic radii to estimate the density in each bin, then it proceeds to fit the density as a function of the radius. A second method uses an analytic property of the NFW profile that relates the maximum of the ratio of the circular velocity to the virial velocity,  $V_{\text{circ}}/V_{\text{vir}}$ . The concentration can be then found as the root of an algebraic equation dependent on this maximum value.

The first method is straightforward to apply but presents two disadvantages. First, it requires a large number of particles in order to have a proper density estimate in each bin. This makes the method robust only for halos with at least  $10^2$  particles. The second problem is that there is not a way to estimate the optimal radial bin size, different choices may produce different results for the concentration.

The second method solves the two problems mentioned above. It works with low particle numbers and does not involve data binning. However, it effectively takes into account only a single data point and discards the rest of the data. Small fluctuations on the maximum can yield large perturbations on the estimated concentration parameter.

In this letter we use bootstrapping to estimate the bias and standard deviation on the concentration estimates as a function of particle number. We show that the two standard methods to estimate concentrations have increasing biases for decreasing particle numbers.

This motivates us to present a third alternative based on fitting the integrated mass profile. This approach has two advantages with respect to the above mentioned methods. It does not involve any data binning and does not throw away data points. This translates into a robust estimate even at low resolution/particle numbers. Furthermore, since the method does not require any binning, there is no need to tune numerical parameters. This is a new independent method to estimate the concentration

parameter.

## 2. BASIC PROPERTIES OF THE NFW DENSITY PROFILE

Let us review first the basic properties of the NFW density profile. This shall help us to define our notation.

### 2.1. Density profile

The NFW density profile can be written as

$$\rho(r) = \frac{\rho_c \delta_c}{r/r_s (1 + r/r_s)^2}, \quad (1)$$

where  $\rho_c \equiv 3H^2/8\pi G$  is the Universe critical density,  $H$  is the Hubble constant,  $G$  and the universal gravitational constant,  $\delta_c$  is the halo dimensionless characteristic density and  $r_s$  is the scale radius. This radius marks the point where the logarithmic slope of the density profile is equal to -2, the transition between the power law scaling  $\rho \propto r^{-1}$  for  $r < r_s$  and  $\rho \propto r^{-3}$  for  $r > r_s$ .

We define the virial radius of a halo,  $r_v$ , as the boundary of the spherical volume that encloses a density of  $\Delta_h$  times the mean density of the Universe. The corresponding mass  $M_v$ , the virial mass, can be written as  $M_v = \frac{4\pi}{3} \bar{\rho} \Delta_h r_v^3$ . From these virial quantities we define new dimensionless variables for the radius and mass  $x \equiv r/r_v$  and  $m \equiv M(< r)/M_v$ .

In this letter we use  $\Delta_h = 740$ , a number roughly corresponding to 200 times the critical density at redshift  $z=0$ .

### 2.2. Integrated mass profile

From these definitions we can compute the total mass enclosed inside a radius  $r$ :

$$M(< r) = 4\pi \rho_c \delta_c r_s^3 \left[ \ln \left( \frac{r_s + r}{r_s} \right) - \frac{r}{r_s + r} \right], \quad (2)$$

or in terms of the dimensionless mass and radius variables

$$m(< x) = \frac{1}{A} \left[ \ln(1 + xc) - \left( \frac{xc}{xc + 1} \right) \right], \quad (3)$$

where

$$A = \ln(1 + c) - \left( \frac{c}{c + 1} \right), \quad (4)$$

and the parameter  $c$  corresponds to the concentration  $c \equiv r_v/r_s$ .

From this normalization and for later convenience we define the following function

$$f(x) = \ln(1 + x) - \left( \frac{x}{x + 1} \right). \quad (5)$$

The most interesting feature of Eq. (3) is that the concentration is the only free parameter to describe the integrated mass profile.

### 2.3. Circular velocity profile

It is also customary to express the mass of the halo in terms of the circular velocity  $V_c = \sqrt{GM(< r)/r}$ . From this we can define a new dimensionless circular velocity  $v(< x) \equiv V_c(< r)/V_c(< r_v)$ , using the result in Eq. 3 we have:

$$v(< x) = \sqrt{\frac{1}{A} \left[ \frac{\ln(1 + xc)}{x} - \frac{c}{xc + 1} \right]}, \quad (6)$$

This normalized profile always shows a maximum provided that the concentration is larger than  $c > 2$ . It is possible to show that for the NFW profile the maximum is provided by

$$\max(v(< x)) = \sqrt{\frac{c}{x_{\max}} \frac{f(x_{\max})}{f(c)}}, \quad (7)$$

where  $x_{\max} = 2.163$  (Klypin et al. 2016) and the function  $f(x)$  corresponds to the definition in Eq. (5).

## 3. METHODS TO ESTIMATE THE CONCENTRATION FROM N-BODY SIMULATIONS

### 3.1. Estimates from the density and velocity profiles

To date, there are two standard methods to estimate concentrations in dark matter halos extracted from N-body simulations. The first method takes all the particles in the halo and bins them in the logarithm of the radial coordinate from the halo center. Then, it estimates the density in each logarithmic bin. At this point is possible to make a direct fit to the density as a function of the radial coordinate. This method has been broadly used for more than two decades to study the mass-concentration-redshift relation of dark matter halos. A second method uses the circular velocity profile. It finds the value of  $x$  for which the normalized circular velocity  $v(< x)$  shows a maximum. Using this value it solves numerically for the corresponding value of the concentration using Eq. (7).

### 3.2. Estimate from the integrated mass profile

Here we propose a new method to estimate the concentration. It uses the integrated mass profile defined in Eq. (3). We build it from N-body data as follows. First, we define the center of the halo to be at the position of the particle with the lowest gravitational potential. Then we rank the particles by their increasing radial distance from the center. From this ranked list of  $i = 1, N$  particles, the total mass at a radius  $r_i$  is  $M_i = i \times m_p$ , where  $r_i$  is the position of the  $i$ -th particle and  $m_p$  is the mass of a single computational particle. We then divide the enclosed mass  $M_i$  and the radii  $r_i$  by their virial values to finally obtain the dimensionless variables  $m_i$  and  $x_i$ .

Using bootstrapping data (§5.1) we find that at a given normalized radius,  $x$ , the logarithm of the normalized integrated mass,  $m$ , approximately follows a Gaussian distribution with variance

$$\sigma_x^2 = \frac{1 - x}{x} \frac{1}{N}. \quad (8)$$

If the integrated mass values at different radii were independent from each other we could write a likelihood distribution as  $\mathcal{L}(c|x_i) \propto \exp(-\chi^2(c, x_i)/2)$  with

$$\chi^2(c, x_i) = \sum_{i=2}^{N-1} \frac{[\log m_i - \log m(< x_i; c)]^2}{\sigma_i^2}, \quad (9)$$

where  $\sigma_i^2 = \sigma_x^2(x_i)$ ,  $m(< x_i; c)$  corresponds to the values in Eq.(3) at  $x = x_i$  for a given value of the concentration

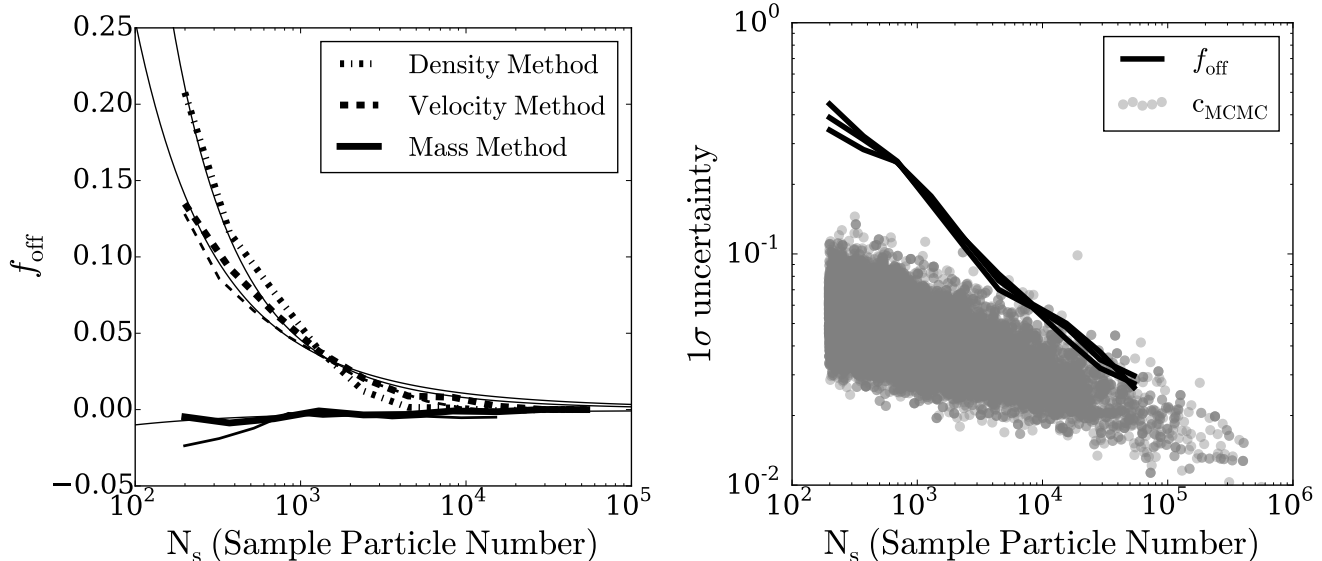


FIG. 1.— *Left panel.* Bias estimated via bootstrapping on the concentration as a function of particle number. Thick (thin) lines correspond to massive halos in the Bolshoi (Via Lactea) simulation. The density method noticeably overestimates the concentration up to a factor of 20%, while the new method only underestimates the concentrations by less than 3%. *Right panel.*  $1\sigma$  uncertainties on the bootstrapped halos (lines) and the MCMC uncertainties on the concentration estimates for each halo using the integrated mass method (circles). Lines show the width between the 14 and 86 percentiles of the  $f_{\text{off}}$  distribution at fixed particle number. The lines include the results for the three methods using Bolshoi data. To allow a fair comparison against  $f_{\text{off}}$ , the MCMC uncertainty has been normalized by the preferred concentration value for each halo.

parameter  $c$ , and the  $i$  index sums over all the particles in the numerical profile. In this computation the particles  $i = 1$  and  $i = N$  are discarded to avoid divergent terms in the sum.

However, tests on the bootstrapping data show that using  $\sigma_i^2 = \sigma_x^2(x_i)$ , instead of the full inverse covariance matrix, grossly overestimates  $\chi^2(c, x_i)$ , providing small uncertainties around the best concentration value. To avoid the expensive computation and inversion of a full covariance matrix we use the bootstrapping data to calibrate an effective  $\sigma_i^2 \approx \sigma_{\text{eff}}^2(x_i)$ .

We impose two conditions on the approximate  $\sigma_{\text{eff}}^2$ . It must keep the dependence on  $x$  that we have discovered for the diagonal elements and must give similar curves of  $\chi^2(c, x_i)$  vs.  $c$  around the minimum as the full covariance matrix. We found that the effective  $\sigma_{\text{eff}}^2$  can be approximated as

$$\sigma_{\text{eff}}^2 = \frac{1-x}{x} \frac{N^{1.15}}{4.5 \times 10^3}. \quad (10)$$

We then use an Affine Invariant Markov Chain Monte Carlo (MCMC) implemented in the python module `emcee` (Foreman-Mackey et al. 2013) to sample the likelihood function distribution. From the  $\chi^2$  distribution we find the optimal concentration value and its associated uncertainty. We stress that different choices for  $\sigma_{\text{eff}}^2$  do not affect the optimal concentration value, only its uncertainty.

Run-time is roughly proportional to  $N$ . Using a single 2.3Ghz CPU core with two walkers over 500 steps takes  $\sim 0.5$  milliseconds per halo per particle in the halo, i.e. a halo with  $N = 2 \times 10^3$  can be fit in one second.

#### 4. NUMERICAL SIMULATIONS AND HALO SAMPLES

We use two different simulations to test our methods. The first is the Bolshoi run, a cosmological simulation

that follows the non-linear evolution of a dark matter density field sampled with  $2048^3$  particles over a cubic box of  $250 h^{-1}\text{Mpc}$  on a side. The cosmological parameters use a Hubble parameter  $h = 0.73$ , a matter density  $\Omega_m = 0.3071$  and a normalization of the power spectrum  $\sigma_8 = 0.82$ . The data is publicly available at <http://www.cosmosim.org/>. Details about the structure of the database and the simulation can be found in (Klypin et al. 2011; Riebe et al. 2013).

We use the halos located in a cubic sub-volume of  $100 h^{-1}\text{Mpc}$  on a side containing a total of 64531 objects. From this sample we select all the halos at  $z = 0$  detected with a Friends-of-Friends (FoF) algorithm with more than 300 particles, meaning that the masses are in the interval  $4 \times 10^{10} \leq M_{\text{FoF}}/h^{-1}\text{M}_\odot \leq 10^{14}$ . The FoF algorithm used a linking length of 0.17 times the mean inter-particle distance. This choice translates into an overdensity  $\Delta_h \sim 400 - 700$  dependent on the halo concentration (More et al. 2011).

From this set of particles we follow the procedure spelled out in Section 3 with  $\Delta_h = 740$  to select an spherical region that we redefine to be our halo. This choice makes that the overdensities are fully included inside the original FoF particle group. On the interest of providing a fair comparison against the density method we only report results from overdensities with at least 200 particles ( $2.6 \times 10^{10} h^{-1}\text{M}_\odot$ ).

We also use public data from the Via Lactea simulation project (Diemand et al. 2008). This simulation contains a single isolated halo with a virial mass of the order of  $10^{12} h^{-1}\text{M}_\odot$  simulated using the tree code PKDGRAV (Stadel 2001). The simulation had  $\sim 2 \times 10^8$  particles to resolve this region. The cosmological parameters are different from those in the Bolshoi simulation, with a Hubble parameter  $h = 0.73$ , a matter density  $\Omega_m = 0.238$  and a normalization of the power spectrum  $\sigma_8 = 0.74$ . The data available to the public corresponds

to a downsampled set of  $10^5$  particles, which corresponds to a particle mass of  $2.24 \times 10^7 h^{-1} \text{M}_\odot$ .

## 5. RESULTS

### 5.1. Bootstrapping to estimate biases

We take halos with at least  $10^5$  particles and subsample them by factors of 2 up to  $10^3$ . We measure the concentration at every resampling. We use a two-sample Kolmogorov-Smirnov (KS) test to compare the list of radial distances from each subsample against that of its parent halo. We find that the resulting p-value distribution is flat. This confirms that the radial particle distribution in the bootstrapped halo is consistent with coming from the distribution given by the parent halo.

For every subsample we keep fixed the virial radius and the center found for the high resolution halo. Leaving the virial radius and center free in each bootstrapping iteration has an effect smaller than 1% in the concentration. In the Bolshoi simulation we select 14 massive halos and create 700 subsamples for each one. For the Via Lactea simulation the same halo is subsampled 10000 times.

The average concentration value for the largest number of particles,  $c_{N_{max}}$ , provides a baseline to compare all the other results. We use the following statistic

$$f_{\text{off}} = c_N / c_{N_{max}} - 1, \quad (11)$$

to account for the offset between the concentration at a given downsampled particle number  $c_N$  and the baseline  $c_{N_{max}}$ .

Figure 1 summarizes our results. The plot on the left shows the average value of  $f_{\text{off}}$  as a function of particle number. This can be interpreted as the statistical bias on the concentration estimate. For large enough particle numbers,  $N_s > 4 \times 10^3$  the results of the three algorithms show a bias below the 1% level. For a lower number of particles the results start to deviate. At 200 particles the velocity method overestimates the concentration by a factor 14% while the density method overestimates it by 20%. Around the same sampling scale, the new algorithm shows a more stable behaviour underestimating the concentration only by a factor of 1%-3%. Work that studied the effect of lowering numerical resolution on the same individual halos (Springel et al. 2008) yielded similar values for the concentration across resolutions. That work explored a particle number range  $> 5 \times 10^5$ , completely consistent with our result that the bias can only be evident for particle numbers  $< 4 \times 10^3$ .

The thin lines on the same panel show a fit to the function

$$f_{\text{off}} = \frac{A}{(1 + \log_{10} N_s)^B}, \quad (12)$$

with  $A = 2842 \pm 1900$ ,  $B = 7.96 \pm 0.54$ ;  $A = 239 \pm 131$ ,  $B = 6.23 \pm 0.43$  and  $A = -0.46 \pm 3.49$ ,  $B = 0.79 \pm 1.31$  for the density, velocity and mass method, respectively.

The right panel in Figure 1 shows different uncertainty results. The lines show the difference between the 14 and 86 percentiles in the  $f_{\text{off}}$  distribution at fixed mass. Each line corresponds to the three different methods to estimate the concentration and the two simulations. This shows that the bootstrapping technique can help us to assign a  $1\sigma$  uncertainty to the concentration values at a

fixed  $N_s$  as

$$\sigma_c = \frac{0.40}{\sqrt{N_s/200}}. \quad (13)$$

The circles in the same Figure show the  $1\sigma$  uncertainty on all the relaxed halos in the Bolshoi simulation sample using the MCMC results. To allow for a fair comparison with the bootstrapping results, this uncertainty is normalized to the concentration value. The uncertainty from the bootstrapping experiment provides an upper bound uncertainty on the concentration estimate for individual halos.

### 5.2. Impact on the Mass-Concentration Relationship

We now inspect the mass-concentration relationship results with the three different algorithms. This can help us to identify possible consequences of the biases detected through the bootstrapping experiments.

Figure 2 shows the mass-concentration relationship for the density, velocity and integrated mass method. The left panel shows the results as they are produced by each of the algorithms. The thin dashed line marks the trend reported by (Prada et al. 2012) using the velocity method, showing that our velocity method implementation can reproduce their results.

The results from the new algorithm follow very closely the velocity algorithm at high masses ( $M_h > 10^{12} h^{-1} \text{M}_\odot$  or equivalently for  $> 4 \times 10^3$  particles). For lower masses there is a difference between the median of the two methods, but they are still consistent within the statistical uncertainties.

We hypothesize that the increase in the results for the velocity and density methods below  $4 \times 10^3$  particles comes from the systematic bias described in the previous section. To test the general consistency of this hypothesis, we correct the concentration values in the velocity and integrated mass methods by a factor of  $1/(1 + f_{\text{off}})$ , using the definition in Equation (11) and the parameters obtained from the data presented in Figure (1). The correction brings into good agreement the results between the velocity/density methods and the new algorithm.

We also notice that the results from the density method have a systematic 15% offset from the velocity methods. This offset was already presented by Prada et al. (2012) for low concentrations ( $c < 6$ ) and high ( $M_h > 10^{12} h^{-1} \text{M}_\odot$ ) halo masses. Recently (Klypin et al. 2016) summarized results for the mass-concentration relationship coming from different methods and datasets to show that similar systematic offsets are present. (Dutton & Macciò 2014) studied the mass-concentration relationship using the maximum velocity and density methods and did not report any significant difference. However, they implemented a modified version of the velocity algorithm that bins the particle data, which might explain why they the offset was not reported.

How do these results impact the most recent mass-concentration estimates? Ludlow et al. (2016) and Klypin et al. (2016) estimated the mass-concentration relation over different suites of cosmological N-body simulations using the density and velocity methods, respectively. Both used halos with at least  $5 \times 10^3$  particles. This imposes a lower halo mass limit of  $\sim 10^{12} h^{-1} \text{M}_\odot$  (Figure 8 in Ludlow et al. (2016), Figure

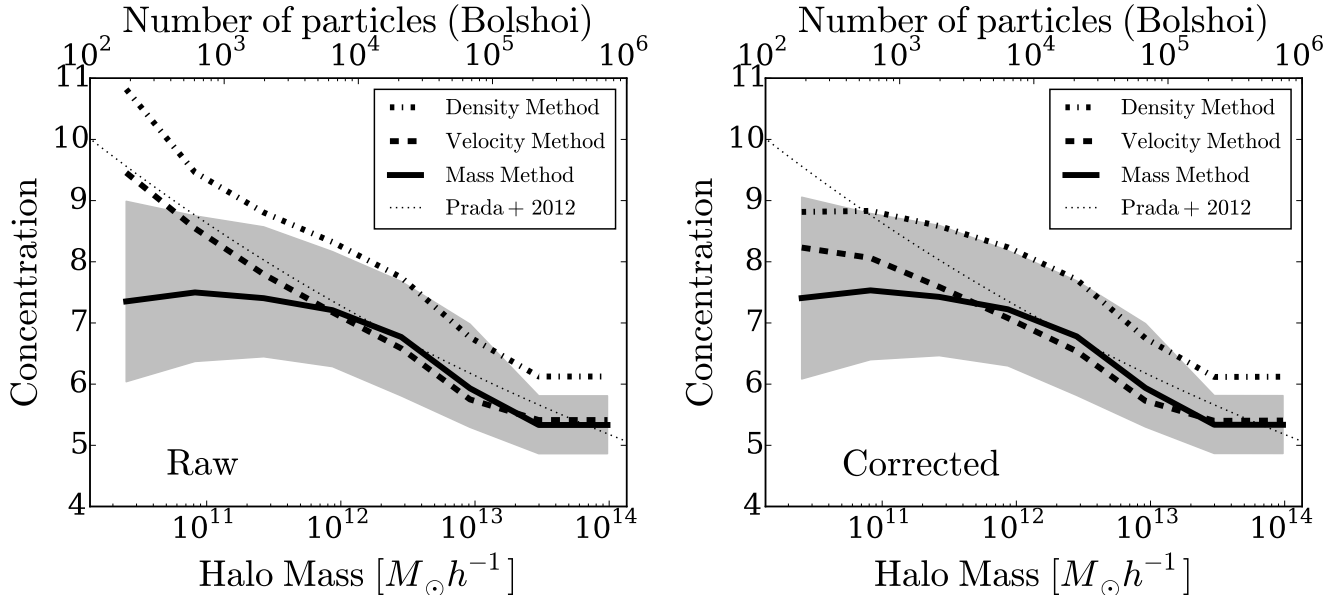


FIG. 2.— Mass-concentration relationship for the three different methods on the Bolshoi data using only relaxed halos. The lines correspond to the median concentration values in each mass bin. The shaded region presents 10 and 90 per cent spread. The three methods have a similar spread but for clarity we only show the spread for the new method. The dotted line corresponds to fits reported by (Prada et al. 2012). The left panel shows the raw results coming from each algorithm. The right panel introduces a correction following the results on the bias as a function of particle number.

17 in Klypin et al. (2016)) to have robust estimates. This means that their results for individual halos should not be affected by the bias we report here. This also leaves open the question about what other methods can robustly say about the flattening we report below  $10^{12} M_{\odot}$  using the new method. However, there are other results at lower masses and higher redshifts (i.e. Prada et al. 2012) that should be reconfirmed using higher resolution simulations as they use halos with only 500 particles.

## 6. CONCLUSIONS

In this letter we used bootstrapping to quantify the biases on concentration estimates. We found that methods commonly used in the literature can overestimate the concentrations by factors of 15%-20% for halos with 200 particles, or 7%-10% for halos with 500 particles. This procedure provides a robust technique to quantify the bias in concentration estimates with the advantage that it works without having to run new simulations.

These results motivated us to introduce a new method based on the integrated mass profile that show a robust performance at low particle numbers. The new algorithm showed a bias of  $< 3\%$  for halos with 200 particles and less than 1% for halos with 500 particles or more. To keep the bias of the velocity and density methods below 2% only halos with at least  $\sim 4000$  particles should be considered.

The three methods are in broad agreement, within the statistical uncertainties, concerning their estimates of the mass-concentration relationship. Some noticeable differences include a 15% systematically higher concentrations in the density method compared to the velocity method. This systematic offset has been reported before with the same dataset (Prada et al. 2012) and with different simulations (Klypin et al. 2016) without any conclusive explanation for its origin. Another difference is that the velocity and integrated mass methods start to differ for masses below  $10^{12} h^{-1} M_{\odot}$  ( $\sim 4000$  particles). We found that correcting the mean concentration by the mean bias factor found through bootstrapping brings these two techniques into agreement.

These results show that using the integrated mass profile to estimate the DM halo concentrations is a tool deserving deeper scrutiny. Further tests with larger simulated volumes, varying numerical resolution, higher redshifts, stacked data and different density profiles are the next natural step to explore the full potential of this new method.

We acknowledge financial support from Uniandes and Universidad de Antioquia. We thank Tomás Verdugo, Stefan Gottloeber and Nelson Padilla for their feedback. We thank the anonymous referees for comments that improved the presentation of these results.

## REFERENCES

- Diemand, J., Kuhlen, M., Madau, P., Zemp, M., Moore, B., Potter, D., & Stadel, J. 2008, *Nature*, 454, 735
- Duffy, A. R., Schaye, J., Kay, S. T., & Dalla Vecchia, C. 2008, *MNRAS*, 390, L64
- Dutton, A. A., & Macciò, A. V. 2014, *MNRAS*, 441, 3359
- Foreman-Mackey, D., Hogg, D. W., Lang, D., & Goodman, J. 2013, *PASP*, 125, 306
- Klypin, A., Yepes, G., Gottlöber, S., Prada, F., & Heß, S. 2016, *MNRAS*, 457, 4340
- Klypin, A. A., Trujillo-Gomez, S., & Primack, J. 2011, *ApJ*, 740, 102
- Ludlow, A. D., Bose, S., Angulo, R. E., Wang, L., Hellwing, W. A., Navarro, J. F., Cole, S., & Frenk, C. S. 2016, *MNRAS*, 460, 1214

- Ludlow, A. D., Navarro, J. F., Angulo, R. E., Boylan-Kolchin, M., Springel, V., Frenk, C., & White, S. D. M. 2014, MNRAS, 441, 378
- Macciò, A. V., Dutton, A. A., & van den Bosch, F. C. 2008, MNRAS, 391, 1940
- More, S., Kravtsov, A. V., Dalal, N., & Gottlöber, S. 2011, ApJS, 195, 4
- Muñoz-Cuertas, J. C., Macciò, A. V., Gottlöber, S., & Dutton, A. A. 2011, MNRAS, 411, 584
- Navarro, J. F., Frenk, C. S., & White, S. D. M. 1997, ApJ, 490, 493
- Navarro, J. F., Ludlow, A., Springel, V., Wang, J., Vogelsberger, M., White, S. D. M., Jenkins, A., Frenk, C. S., & Helmi, A. 2010, MNRAS, 402, 21
- Neto, A. F., Gao, L., Bett, P., Cole, S., Navarro, J. F., Frenk, C. S., White, S. D. M., Springel, V., & Jenkins, A. 2007, MNRAS, 381, 1450
- Prada, F., Klypin, A. A., Cuesta, A. J., Betancort-Rijo, J. E., & Primack, J. 2012, MNRAS, 423, 3018
- Riebe, K., Partl, A. M., Enke, H., Forero-Romero, J., Gottlöber, S., Klypin, A., Lemson, G., Prada, F., Primack, J. R., Steinmetz, M., & Turchaninov, V. 2013, Astronomische Nachrichten, 334, 691
- Springel, V., Wang, J., Vogelsberger, M., Ludlow, A., Jenkins, A., Helmi, A., Navarro, J. F., Frenk, C. S., & White, S. D. M. 2008, MNRAS, 391, 1685
- Stadel, J. G. 2001, PhD thesis, UNIVERSITY OF WASHINGTON